Enhancement of photonic density of states in finite graphene multilayers

Ashley M. DaSilva,[1] You-Chia Chang,[2,3] Ted Norris,[3,4] and Allan H. MacDonald[1]
[1]*Department of Physics, The University of Texas at Austin, Austin, Texas 78712-1192, USA*
[2]*Applied Physics Program, The University of Michigan, Ann Arbor, Michigan 48109, USA*
[3]*Center for Ultrafast Optical Science, The University of Michigan, Ann Arbor, Michigan 48109, USA*
[4]*Department of Electrical Engineering and Computer Science, The University of Michigan, Ann Arbor, Michigan 48109, USA*
(Received 24 July 2013; revised manuscript received 25 September 2013; published 13 November 2013)

We consider the optical properties of finite systems composed of a series of graphene sheets separated by thin dielectric layers. Because these systems respond as conductors to electric fields in the plane of the graphene sheets and as insulators to perpendicular electric fields, they can be expected to have properties similar to those of hyperbolic metamaterials. We show that under typical experimental conditions graphene/dielectric multilayers have enhanced Purcell factors, and enhanced photonic densities of states in both the terahertz (THz) and midinfrared (mid-IR) frequency range. These behaviors can be traced to the coupled plasmon modes of the multilayer graphene system. We show that these results can be obtained with just a few layers of graphene.

DOI: 10.1103/PhysRevB.88.195411 PACS number(s): 78.67.Wj, 78.67.Pt, 73.20.Mf, 81.05.Xj

I. INTRODUCTION

Hyperbolic metamaterials (HMMs) are artificially structured materials that have hyperbolic light dispersion, leading to an enhanced photonic density of states.[1–5] One approach that is used to design a HMM is to consider superlattices with alternating metal and dielectric layers and subwavelength periods. When described as a homogenous material using an effective medium approximation, the dielectric constants of such a superlattice are[6,7]

$$\epsilon_{\parallel} = \rho\epsilon_d + (1-\rho)\epsilon_m, \tag{1}$$

$$\epsilon_{\perp} = \left(\frac{\rho}{\epsilon_d} + \frac{1-\rho}{\epsilon_m}\right)^{-1}, \tag{2}$$

where $\parallel$ and $\perp$ refer to the directions parallel and perpendicular to the interfaces, ρ is the dielectric to metal thickness ratio, and $\epsilon_{d(m)}$ is the dielectric function of the dielectric (metal) constituent. By proper choice of materials, thickness ratio, and frequency, one can engineer a material with a hyperbolic dispersion relation, i.e., a system in which $\epsilon_{\parallel}$ and $\epsilon_{\perp}$ have opposite signs over a wide range of frequencies.

HMMs are important in photonic engineering,[8] especially in applications to subwavelength imaging[9,10] and confinement.[11] Near-field thermal properties may also be engineered using HMMs for applications such as energy harvesting and thermal management.[12] One can also use HMMs to control luminescence via the Purcell effect,[4,13] which reflects the dependence of spontaneous emission on the surrounding density of photonic states. In free space, the density of photonic states is proportional to ω^2. In the presence of an interface, the density of states can be enhanced by evanescent modes close to the interface. The size of the enhancement can be a few orders of magnitude, with most of the states localized close to the interface, leading to a more rapid excited state decay and enhanced photoluminescence of nearby atoms; this is the origin of the Purcell enhancement factor. HMMs can have particularly strongly enhanced photonic densities of states.

There are two types of HMMs depending on which components of the dielectric tensor are negative. Type I HMMs have a metal-like perpendicular dielectric constant ($\epsilon_{\perp} < 0$, $\epsilon_{\parallel} > 0$) while type II HMMs have a metal-like parallel dielectric constant ($\epsilon_{\parallel} < 0$, $\epsilon_{\perp} > 0$). As an alternative to the alternating layer strategy,[5,14] HMMs can also be constructed by embedding metallic nanowires in a dielectric medium.[15,16]

Graphene, a monolayer of graphite, has long-lived long-wavelength plasmons, which are tunable via gate voltage.[17–21] The possibility of gate tuning is one attractive feature of using graphene for the metallic layers in an HMM. Indeed, infinite graphene/dielectric stacks have recently been predicted to have a large Purcell factor and a negative[22] $\epsilon_{\parallel}$ and arrays of graphene ribbons have been predicted to perform favorably as a hyperlens.[23] Recent calculations of Fresnel coefficients and power spectra in the terahertz (THz) frequency regime provide further evidence of graphene's suitability as a component of HMMs.[24] Here, we report a study of finite stacks of graphene layers in both the THz and midinfrared (mid-IR) frequency ranges, and show that even for a small number of layers, graphene/dielectric stacks retain desirable HMM properties, in particular an enhanced photonic density of states.[25] We emphasize that only in systems composed of a small number of graphene sheets will it actually be possible to modify the carrier densities and hence the plasmon frequencies of individual graphene layers via the electric field effect.[26] (Screening prevents a back gate from influencing layers far from the substrate.[27])

We have also found that while having a dielectric between the graphene layers is important in order to prevent interlayer tunneling, its direct role in modulating optical properties in tuning HMM effects for electromagnetic radiation in the THz regime is minimal. We find that graphene HMMs boast a large photonic density of states enhancement for a wide range of frequencies, and that the properties are robust to the dielectric spacer thickness, Fermi energy, and elastic mean free path. We focus on wave-vector-resolved transmission coefficient and photonic density of states, which show the presence of modes within the metamaterial that are evanescent in free space. The enlarged photonic density of states leads to a Purcell enhancement that is greatly improved relative to metal/dielectric layered HMMs.

We note that we have assumed equal carrier densities in all of the graphene layers. This is an unrealistic approximation for multilayer graphene samples utilizing the electric field effect to control the carrier density.[28] However, it is possible to achieve approximately equal carrier densities by using doping techniques,[29,30] and in this case, we expect our assumption to be valid.

Our paper is organized as follows. We first describe the electromagnetic Green's functions and transfer matrices we use to perform calculations. We then characterize graphene HMMs by evaluating the reflection coefficients, showing that the anticipated HMM features are already realized at quite small graphene layer numbers. We then calculate the transmission coefficient and wave-vector-resolved photonic density of states for an $N = 6$-layer graphene-based HMM to illustrate the dependence of various properties on controllable parameters. Finally, we evaluate the photonic density of states and Purcell coefficient for finite graphene-based HMMs in both the THz and the mid-IR regime.

II. THEORETICAL FORMULATION

Maxwell's equations in a uniform medium with dielectric constant ϵ and permittivity $\mu = 1$ are conveniently solved using electromagnetic Green's functions defined by the differential equation[31,32]

$$\nabla \times \nabla \times \overleftrightarrow{G}_0^{\mathrm{EM}}(\mathbf{r}) - \frac{\epsilon\omega^2}{c^2}\overleftrightarrow{G}_0^{\mathrm{EM}}(\mathbf{r}) = \delta(\mathbf{r}). \tag{3}$$

This function is called the dyadic Green's function to reflect the property that a source oriented in one direction can in general result in electric and magnetic (EM) fields in any direction. In free space, the electric and magnetic Green's functions are the same. The electric and magnetic fields are obtained by integrating the electromagnetic Green's functions over the sources:

$$\mathbf{E}(\mathbf{r}) = \frac{4\pi i\omega}{c^2}\int d\mathbf{r}'\,\overleftrightarrow{G}_0^{\mathrm{EM}}(\mathbf{r}-\mathbf{r}')\mathbf{J}(\mathbf{r}'), \tag{4}$$

$$\mathbf{H}(\mathbf{r}) = \int d\mathbf{r}'\,\overleftrightarrow{G}_0^{\mathrm{EM}}(\mathbf{r}-\mathbf{r}')\mathbf{M}(\mathbf{r}'), \tag{5}$$

where $\mathbf{J}$ includes all free currents and $\mathbf{M}(\mathbf{r}) = (4\pi/c)\nabla \times \mathbf{J}(\mathbf{r})$ can be thought of as the magnetization they produce.

The electromagnetic local density of states (LDOS) can also be calculated from the Green's function[31–33]

$$\rho(\omega,z) = \frac{\omega}{\pi c^2}\mathrm{Im\ tr}\,\overleftrightarrow{G}, \tag{6}$$

where Im denotes the imaginary part and tr denotes the trace. In our planar geometry, ρ depends only on the coordinate z, which measures position relative to the graphene/dielectric multilayer. In a nonuniform medium, the electric and magnetic Green's functions will be different, and the total density of states is the sum of the electric and magnetic components, $\rho(\omega,z) = \rho^E(\omega,z) + \rho^H(\omega,z)$.[31]

The Green's functions defined in Eq. (3) are those of a uniform medium, while the expression for the LDOS (6) depends on the Green's function in the nonuniform medium. We will assume that the top surface of an HMM of total thickness L is located at $z = 0$, and the regions $z > 0$ and $z < -L$ are free space ($\epsilon = 1$). The presence of the HMM can then be accounted for by writing the total electromagnetic field at $z > 0$ as the sum of the incident and reflected parts. We find that the electric Green's function for $z > 0$ can then be written as

$$\begin{aligned}\overleftrightarrow{G}^{E}(k,z,z';\omega) = \frac{i}{2K}[&(\hat{s}\hat{s} + \hat{p}_-\hat{p}_-)e^{-iK(z-z')}\theta(z'-z)\\ &+(\hat{s}\hat{s} + \hat{p}_+\hat{p}_+)e^{iK(z-z')}\theta(z-z')\\ &+(r_s\hat{s}\hat{s} + r_p\hat{p}_+\hat{p}_-)e^{iK(z+z')}],\end{aligned} \tag{7}$$

where k is the two-dimensional in-plane wave vector, $K = \sqrt{\epsilon\omega^2/c^2 - k^2}$ is the out-of-plane wave vector, and r_α for $\alpha = s,p$ are the reflection coefficients for the two polarizations of EM waves. Here and below, we set ϵ to 1 for an HMM embedded in a vacuum. The polarization vectors are

$$\hat{s} = \frac{1}{k}(k_y\hat{x} - k_x\hat{y}),$$

$$\hat{p}_\pm = \frac{1}{\sqrt{k^2+K^2}}(\mp K\hat{k} + k\hat{z}),$$

denoting s (TE) and p (TM) polarized light. The $\pm$ index on $\hat{p}$ distinguishes upward moving and downward moving waves. The magnetic Green's function can be obtained from the electric Green's function by replacing $r_s \leftrightarrow r_p$.[31] We now see that the Green's function for $z > 0$, and therefore the LDOS, is determined solely by the reflection coefficients. The LDOS is

$$\rho(\omega,z) = \frac{\omega}{\pi c^2}\mathrm{Re}\left\{\int\frac{dk}{2\pi}\frac{k}{2K}\left[4+\frac{4k^2}{\epsilon\omega^2/c^2}(r_s+r_p)e^{2iKz}\right]\right\}, \tag{8}$$

where $K = \sqrt{\omega^2/c^2 - k^2}$ and $\epsilon = 1$ when the HMM is in vacuum. The reflection coefficients, r_s and r_p, are functions of k and are explicitly provided below.

Below we also consider the wave-vector resolved LDOS, $\rho(q,\omega,z)$, which separates contributions to the LDOS from different wave vectors:

$$\rho(k,\omega,z) = \frac{\omega}{\pi c^2}\mathrm{Re}\left\{\frac{2}{K}\left[1+\frac{c^2k^2}{\epsilon\omega^2}(r_s+r_p)e^{2iKz}\right]\right\}. \tag{9}$$

The vacuum LDOS can be recovered by setting the reflection coefficients to zero:

$$\rho_0(k,\omega,z) \equiv \rho_0(k,\omega) = \frac{2\omega}{\pi c^2}\frac{\theta(\omega/c-k)}{\sqrt{\epsilon\omega^2/c^2-k^2}}, \tag{10}$$

$$\rho_0(\omega,z) \equiv \rho_0(\omega) = \frac{\omega^2}{\pi^2c^3}, \tag{11}$$

which are independent of z. Note that in the absence of an interface, there is no contribution to the DOS from wave vectors $k > \omega/c$.

The reflection coefficients r_s and r_p for s- and p-polarized light, respectively, are defined as the ratio of the reflected to the incident electromagnetic field at the interface. They are determined entirely by the boundary conditions imposed by Maxwell's equations:

$$\begin{pmatrix}E_{2\uparrow}\\ E_{2\downarrow}\end{pmatrix} = M_{12}^{s(p)}\begin{pmatrix}E_{1\uparrow}\\ E_{1\downarrow}\end{pmatrix}, \tag{12}$$

where the indices 1 and 2 refer to the region above and below a graphene sheet, and ↑ and ↓ denote the upward moving and downward moving modes, respectively. The matrices connecting the fields are

$$M_{12}^{s} = \frac{1}{2}\begin{pmatrix} 1+\frac{Q_1}{Q_2}-\frac{4\pi\sigma\omega}{c^2Q_2} & 1-\frac{Q_1}{Q_2}-\frac{4\pi\sigma\omega}{c^2Q_2} \\ 1-\frac{Q_1}{Q_2}+\frac{4\pi\sigma\omega}{c^2Q_2} & 1+\frac{Q_1}{Q_2}+\frac{4\pi\sigma\omega}{c^2Q_2} \end{pmatrix}, \quad (13)$$

$$M_{12}^{p} = \frac{1}{2}\begin{pmatrix} 1+\frac{\epsilon_2 Q_1}{\epsilon_1 Q_2}+\frac{4\pi\sigma Q_1}{\omega\epsilon_1} & 1-\frac{\epsilon_2 Q_1}{\epsilon_1 Q_2}-\frac{4\pi\sigma Q_1}{\omega\epsilon_1} \\ 1-\frac{\epsilon_2 Q_1}{\epsilon_1 Q_2}+\frac{4\pi\sigma Q_1}{\omega\epsilon_1} & 1+\frac{\epsilon_2 Q_1}{\epsilon_1 Q_2}-\frac{4\pi\sigma Q_1}{\omega\epsilon_1} \end{pmatrix}. \quad (14)$$

The two-dimensional conductivity of a graphene is given by[34–40]

$$\sigma(\omega) = \frac{2e^2}{h}\left[i\frac{\varepsilon_F}{\hbar\omega + i\hbar/\tau} + \frac{i}{4}\ln\left|\frac{\hbar\omega - 2\varepsilon_F}{\hbar\omega + 2\varepsilon_F}\right| + \frac{\pi}{4}\theta(\hbar\omega - 2\varepsilon_F)\right]. \quad (15)$$

Here, v_D is the Dirac velocity of graphene, $\varepsilon_F = \hbar v_D\sqrt{\pi n}$ is the Fermi energy as a function of carrier density n, τ is the transport time (which depends on the mobility), and $\theta(x)$ is the step function that specifies the threshold for interband transitions at large ω. This expression ignores the nonlocal response and is appropriate for $k \to 0$. In practice, this expression is found to work well away from the onset of interband transitions, which occurs when $\hbar\omega \approx 2E_F$.[40] Inserting a transfer matrix for each graphene layer, and one propagation matrix

$$P_i = \begin{pmatrix} e^{-iQ_i d_i} & 0 \\ 0 & e^{iQ_i d_i} \end{pmatrix} \quad (16)$$

for each dielectric layer of thickness d_i, the total transfer matrix is a product of the component matrices,

$$M^{s(p)} = \prod_j P_j M_{j-1,j}^{s(p)}. \quad (17)$$

The reflection coefficient $r_{s(p)}$ and transmission coefficient $t_{s(p)}$ are obtained from these expressions by solving

$$\begin{pmatrix} 0 \\ t_{s(p)} \end{pmatrix} = M^{s(p)}\begin{pmatrix} r_{s(p)} \\ 1 \end{pmatrix}. \quad (18)$$

III. OPTICAL PROPERTIES

The Purcell enhancement factor is defined as the ratio of the total radiation rate of a unit dipole source to the radiation rate of the dipole in vacuum:[7,41]

$$b = 1 + \frac{3}{2\omega/c}\mathrm{Re}\left\{\int_0^\infty \frac{dk\,k}{K}\left[f_\perp^2\frac{k^2 r_p}{\omega^2/c^2} + \frac{1}{2}f_\parallel^2\left(r_s - \frac{K^2}{\omega^2/c^2}\,r_p\right)\right]e^{2iKz}\right\}, \quad (19)$$

where z is the surface to dipole distance, and $f_\parallel$ and $f_\perp$ are the components of the dipole along the directions parallel and perpendicular to the HMM layers, respectively.

In the effective medium approximation, the enhanced Purcell effect can be traced to the nonzero imaginary part of the reflection coefficient in the large k limit, $k/(\omega/c) \to \infty$.[7] In real systems, the finite period of the HMM limits the maximum value of k, but the signature of a nonzero imaginary part of the reflection coefficient for $k > \omega/c$ remains. These modes are evanescent in the vacuum on either side of the system, but propagate within the structure, as demonstrated by the enhanced transmission coefficient.[42]

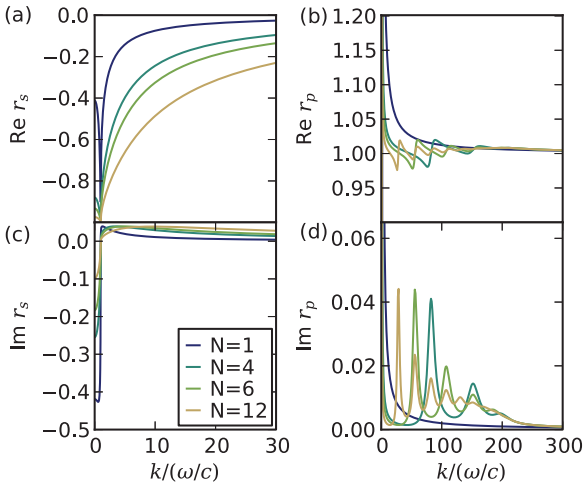

FIG. 1. (Color online) Real (top) and imaginary (bottom) parts of the reflection amplitudes for s (left) and p (right) polarized EM waves on graphene HMMs with different numbers of layers N. The parameters used for this calculation were frequency $f = 1.0$ THz ($\hbar\omega = 4.1$ meV), $n = 4 \times 10^{12}$ cm^{-2} (Fermi energy $E_F = 0.23$ eV) in every layer, $\mu = 50{,}000$ cm^2/Vs for graphene, $d = 10$ nm for the dielectric layer thicknesses, and $\epsilon = 3.9$ for their dielectric constant.

In Fig. 1, we plot the reflection coefficients for s- and p-polarized light as a function of wave vector normalized to frequency. For s-polarized light, the number of graphene layers has little effect. For p-polarized light, a greater number of layers leads to more peaks of smaller magnitude while the general features remain intact, including the presence of a nonzero imaginary part of the reflection coefficient up to $k \sim 200\omega/c$. For the same parameters, Fig. 2 shows the

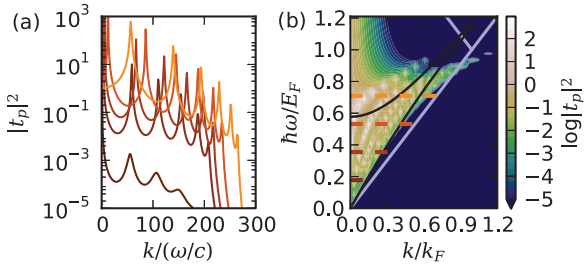

FIG. 2. (Color online) (a) Magnitude squared of the transmission amplitudes for p-polarized light on six layers of graphene HMM with the same material parameters as in Fig. 1 and ω ranging from $\hbar\omega = 4.0$ meV ($f = 1.0$ THz) to $\hbar\omega = 165$ meV ($f = 40$ THz), corresponding to the frequencies shown as colored lines in (b). (b) The logarithm of the magnitude squared of the transmission coefficient is shown as a function of frequency in units of Fermi energy and wave vector in units of Fermi wave vector. The Fermi energy is 233 meV. Overlayed on this plot are the threshold frequencies for interband transitions (solid grey lines) and the frequency range of bulk plasmons in graphene superlattices (solid black lines).

transmittance versus parallel wave vector. Various values of frequency ω are considered. For both s- and p-polarized light, a significant fraction of the electromagnetic wave is transferred through the structure at $k < \omega/c$. This is due to the fact that the wavelength is much larger than the total thickness, $\lambda \gg Nd$, for $N = 6$ layers each of thickness $d = 10$ nm. We also observe finite transmission when $k > \omega/c$ for both polarizations. As the frequency increases, the high-k transmission coefficient decays more rapidly for s-polarized radiation compared to p-polarized radiation. This decay is due to the decreased wavelength, and is similar to the behavior of a uniform dielectric. On the other hand, the transmission coefficient for p-polarized radiation has several sharp peaks when $k > \omega/c$. A large value of $|t_p|^2$ corresponds to $t = E_{2\downarrow}/E_{1\downarrow} > 1$. When $k > \omega/c$, the $\uparrow$ ($\downarrow$) labels correspond to the evanescent modes which decay to zero for $z \to -\infty$ and $z \to +\infty$, respectively. Any electromagnetic mode with $k > \omega/c$ must decay in the free space on either side of the HMM, so $E_{1\uparrow} \to 0$, yielding peaks at electromagnetic modes of the HMM.

The peaks in transmission for p-polarized radiation are obtained in the same regime where there are peaks in the imaginary part of the reflection coefficient (see Fig. 2). Such features are not observed for s-polarized radiation, which does not excite plasmon resonances since the electric field and parallel wave vector are perpendicular. These peaks reflect the coupled plasmon modes in the graphene layers,[43] which have energies bounded by the dashed black lines in Fig. 2(b). These modes have been predicted and observed in 2DEG superlattices previously,[44–48] and are usually discussed in terms of instantaneous intra and interlayer Coulomb interactions, an approximation that is reliable in the large k regime. In the context of HMMs, these are sometimes called high-k propagating modes[42] and have application in subwavelength confinement and imaging.[9] As the frequency is increased, the transmission of p-polarized radiation is enhanced, with an optimal value at around 40 THz (165 meV), close to the Fermi energy. For frequencies above the Fermi energy, the photon energy is above the maximum plasmon energy,[43,45,46,48] and all high-k modes disappear.

The desirable properties of HMMs stem from their enhanced LDOS at wave vector $k > \omega/c$. The LDOS will be a function of frequency ω and distance z above the graphene HMM. The wave-vector-resolved LDOS is shown in Fig. 3 for the same parameters as in Figs. 1 and 2 and for two different values of the distance z. As expected, the LDOS at large z (dashed lines) decays more rapidly at large wave vector due to the weak influence of evanescent modes far from the surface of the HMM. We also notice that the LDOS enhancement is greater for smaller frequencies, in spite of the opposite trend in the transmission coefficient for p polarization [see Fig. 2(b)]. This is also an expected trend, and is due to the $1/\omega$ dependence of the LDOS, which is apparent in the Purcell factor, Eq. (19). In addition to the overall larger LDOS, the peaks in the LDOS are smeared out for smaller frequencies because $\hbar\tau^{-1} \approx 0.7$ meV is held constant.

One must be careful at large wave vectors ($k \approx k_F$) where the local approximation for the conductivity of graphene, Eq. (15), becomes questionable.[34] We have found that the LDOS decays before reaching $k = k_F$ for frequencies above $\approx$4 meV at 10 nm, and for all frequencies studied here

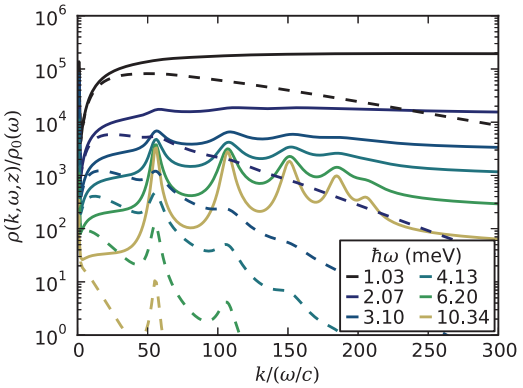

FIG. 3. (Color online) The LDOS for a six layer graphene HMM with the same material parameters as Fig. 1 and different values of ω ranging from $\hbar\omega = 1.03$ meV ($f = 0.25$ THz) to $\hbar\omega = 10.34$ meV ($f = 2.5$ THz), corresponding to the frequencies shown in the legend. The solid and dashed lines correspond to distances of $z = 10$ nm and 1000 nm above the surface of the HMM, respectively. Values of $(\omega/c)\ell_{\rm mfp} \approx 0.003$ to 0.03 for frequencies shown on this plot.

at 1 μm. At smaller frequencies and distances close to the interface, the calculation may become unreliable unless nonlocal corrections to the conductivity are made. Nonlocal effects are known to provide a large wave-vector cutoff of the LDOS enhancement.[49] In the ballistic limit, $k\ell_{\rm mfp} \gg 1$ ($\ell_{\rm mfp}$ is the elastic mean-free path for electrons), nonlocal effects are important when $\omega > v_D k$, where v_D is the Dirac velocity of electrons. This limit reduces to $k/(\omega/c) < 300$.

The other parameters in the model are the period of the graphene/dielectric superlattice, the carrier density, and the mobility of the graphene sheets. For simplicity, we have assumed that all graphene sheets have the same carrier density and mobility. The former assumption is unrealistic when carriers are induced by gates, as mentioned previously, but does not influence properties in an essential way. Figure 4(a) shows the dependence of the LDOS on both wave vector and period d. The calculations were performed for a distance of $z = 50$ nm from the surface. The LDOS is only weakly dependent on d for features at small k; this is because for the THz regime under consideration, d is always much smaller than λ ($\lambda \sim 100$ μm for the frequencies studied here). However, there is a noticeable enhancement of the high-k features in the LDOS as d decreases due to the dependence of the transfer matrix on the combination kd, which becomes comparable to 1 at $k/(\omega/c) \sim 500$ for $d = 10$ nm and $k/(\omega/c) \sim 5000$ for $d = 1$ nm. Figure 4(b) shows the logarithm of the LDOS versus Fermi energy and $k/(\omega/c)$. The dependence again is weak, but as the Fermi energy decreases, there is an enhancement when ω becomes comparable to E_F. For smaller Fermi energies, we expect that our local approximation for $\sigma(\omega)$ breaks down. In realistic multilayers that have carriers induced by gates, the density will normally be low in some layers. Figure 4(c) shows the logarithm of the LDOS *vs* $\hbar\tau^{-1}$ and $k/(\omega/c)$. Again, the dependence is relatively weak, however, there is a noticeable enhancement of the LDOS as τ decreases. This is probably due to stronger absorption in the graphene planes as the real part of the conductivity becomes larger.

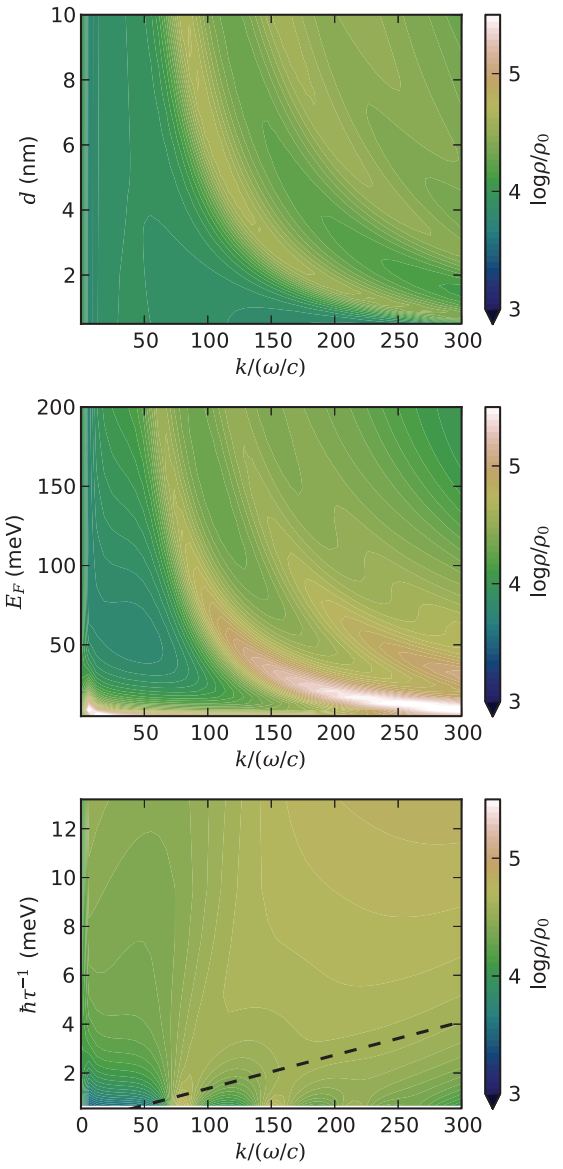

FIG. 4. (Color online) The logarithm of the LDOS at $z = 50$ nm as a function of parallel wavevector divided by vacuum wavevector, $k/(\omega/c)$, and (a) the distance between graphene sheets, d, for fixed Fermi energy $E_F = 234$ meV and relaxation time $\tau = 10^{-12}$ s; (b) Fermi energy, E_F, for fixed $d = 10$ nm and $\tau = 10^{-12}$ s; (c) inverse relaxation time, τ^{-1} for fixed $E_F = 234$ eV and $d = 10$ nm. For all plots, $\hbar\omega = 4.1$ meV and there are six layers of graphene separated by a dielectric with $\epsilon = 3.9$. The dashed line in (c) corresponds to $k\ell_{\text{mfp}} = 1$. In (a) and (b), $k\ell_{\text{mfp}} = 3.7$ on the right-hand side of the figure.

The Purcell factor depends not on the wave-vector-resolved LDOS, but on the total LDOS, integrated over all wave vectors. In Fig. 5(a), we show the integrated LDOS normalized to the vacuum LDOS versus z for different values of ω. As expected, the normalized LDOS decays away from the surface, and will reach a value of 1 for $z \gg \lambda$. We also see that the normalized LDOS is larger for smaller values of ω. Figure 5(b) shows the dependence of the normalized LDOS as a function of both z and ω for six layers of graphene with $n = 4 \times 10^{12}$ cm^{-2}. We

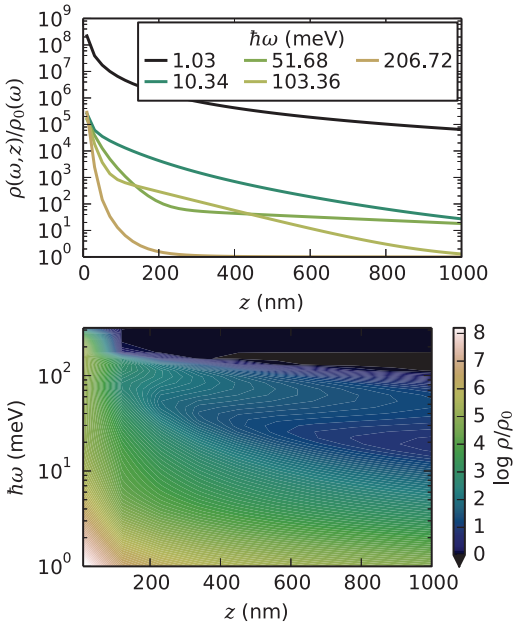

FIG. 5. (Color online) (a) The integrated LDOS as a function of z for several values of ω as indicated in the legend. (b) The logarithm of the integrated LDOS as a function of ω and z. For both (a) and (b), the system is six layers of graphene with $n = 4 \times 10^{12}$ cm^{-2} and $\mu = 50\,000$ cm^2/Vs separated by 10 nm of dielectric with $\epsilon = 3.9$.

again note that for small ω our local approximation for the conductivity of graphene is questionable.

Next, we calculate the Purcell factor of a ten-layer graphene HMM (total thickness 100 nm) for the parameters $\hbar\omega = 4.1$ meV, $n = 4 \times 10^{12}$ cm^{-2}, $\mu = 50\,000$ cm^2/Vs, and $\epsilon = 3.9$. Figure 6 shows the Purcell factor calculated for the two orientations of a unit dipole: perpendicular to the surface

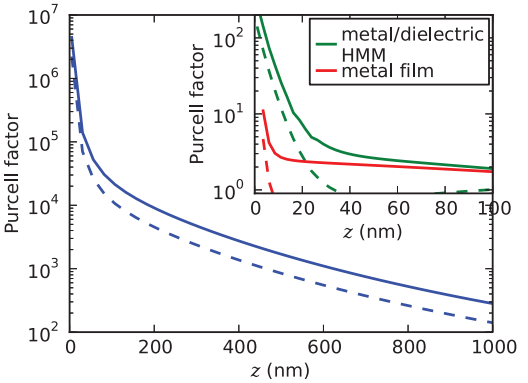

FIG. 6. (Color online) The Purcell factor as a function of z for a graphene HMM. The inset shows the Purcell factor as a function of z for a metal/dielectric HMM and a metallic film. All three have 100 nm total thickness. The graphene HMM is composed of ten layers of 10 nm each, having the same parameters as in Fig. 5 and at $\hbar\omega = 4.1$ meV. The metal/dielectric HMM has ten unit cells each composed of 5 nm of metal ($\epsilon_m = -27.5 + 0.31i$) and 5 nm of dielectric ($\epsilon_d = 6.7$), and is at a frequency of $\hbar\omega = 1.65$ eV. The metallic film has the parameters of the metallic part of the metal/dielectric HMM and is at the same frequency. In both the main figure and the inset, the solid lines are for a dipole oriented parallel to the HMM layers and the dashed lines are for a dipole perpendicular to the HMM layers.

(dashed) and parallel to the surface (solid lines). In the inset of Fig. 6, we show the calculation of the Purcell factor for 100 nm of both a metal/dielectric HMM (green) and metallic film (red). The metal/dielectric HMM is composed of ten unit cells of 5 nm of metal with dielectric constant $\epsilon_m = -27.5 + 0.31i$, and 5 nm of dielectric with dielectric constant $\epsilon_d = 6.7$ at a wavelength of 750 nm, parameters which are relevant for Ag/TiO_2 multilayers, which have been used as typical HMMs for experiments and theory.[42,50,51] The metallic film has the parameters for the metal at the same wavelength. Our results for the Purcell enhancement versus dipole distance are in agreement with those obtained in Ref. 24 for a semi-infinite graphene-based HMM. We find that the Purcell factor for graphene is enhanced at small distances compared to both the metal/dielectric HMMs and the metal films. However, one must note that the wavelength of the metal/dielectric HMM is necessarily different than the wavelength of the graphene HMMs. Metal/dielectric HMMs are limited to a frequency regime where the metal has a negative dielectric response (typically in the optical region of the electromagnetic spectrum), while the graphene HMMs are limited by the Fermi energy (typically in the THz to mid-IR region.) Note, for example, at $z = 1$ nm, the metal/dielectric HMM has a Purcell factor $\sim 10^2$. Keeping the ratio of z to free space wavelength $\lambda = 2\pi c/\omega$ for the two metamaterials the same, the corresponding value of z for the graphene-based HMM is $z \approx 400$ nm. We observe that the Purcell factor is $\sim 10^3$, a factor of 10 enhancement compared to the metal/dielectric HMM.

One obtains a large Purcell enhancement at small distances for small numbers of graphene layers. Figure 7 shows a comparison of the Purcell factor for $N = 1$, 2, 4, 6, and 10 layers of graphene. For one or two graphene layers, the Purcell factor decays more rapidly. By the time, there are four graphene layers, the curves are almost identical up to $z = 1000$ nm.

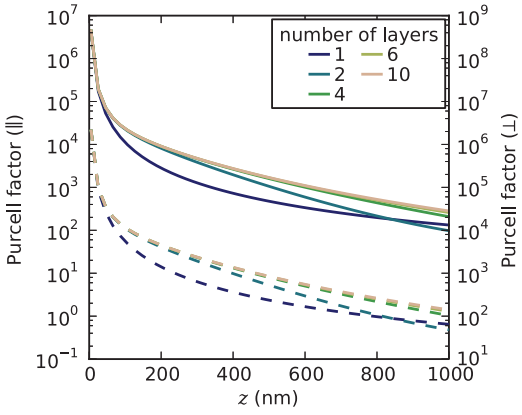

FIG. 7. (Color online) The Purcell factor as a function of z for a graphene HMM of 1, 2, 4, 6, and 10 layers, as denoted in the legend. The Purcell factors for parallel and perpendicular dipoles have been plotted against different axes for clarity. Solid lines correspond to a dipole oriented parallel to the surface, with Purcell enhancement given on the left axis, while dashed lines correspond to a dipole oriented perpendicular to the surface, with Purcell enhancement given on the right axis. The parameters of the graphene and dielectric are the same as in Fig. 5 and at $\hbar\omega = 4.1$ meV.

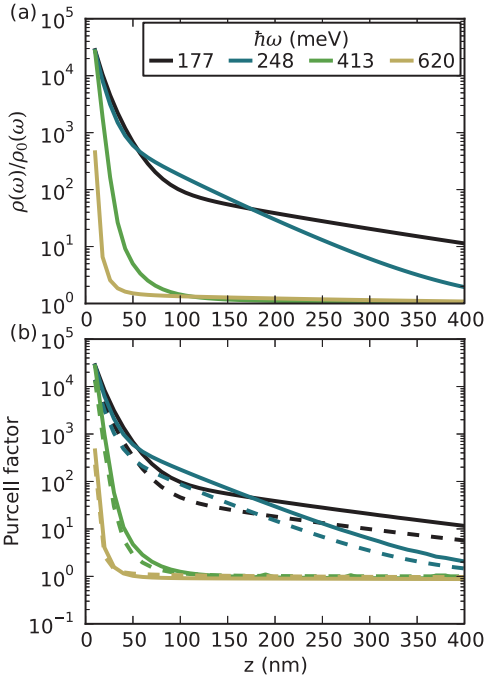

FIG. 8. (Color online) Properties of a highly doped, low mobility graphene HMM in the mid-IR regime. In both panels, the graphene layers are separated by 10 nm of dielectric with $\epsilon = 3.9$. The graphene layers have a carrier density of 5×10^{13} cm^{-2} and a mobility of $\mu = 1000$ cm^2/Vs. (a) The integrated local density of states as a function of position z above the top graphene layer. The wavelengths range from 3 to 8 μm, with energies $\hbar\omega$ indicated in the legend. (b) The Purcell factor of a unit dipole oriented parallel (solid) and perpendicular (dashed) to the surface of a ten-layer graphene metamaterial. The frequency of the oscillating dipole corresponds to those noted in the legend of (a).

This shows that graphene-based hyperbolic metamaterials are possible for few layers of graphene, as low as $N = 4$.

So far, our calculations are for high-mobility graphene layers typical of exfoliated samples. Graphene grown by chemical vapor deposition (CVD) tends to have a lower mobility around 1000 cm^2/Vs. For such samples, it is beneficial to operate in the mid-infrared (mid-IR) regime, where the conductivity given by Eq. (15) will still have a significant imaginary part despite the smaller relaxation time. Since the frequency regime for the HMM is limited by the Fermi level, it is necessary for such samples to be highly doped, to 10^{13} cm^{-2} or larger carrier density. We have calculated the integrated LDOS and Purcell factor for highly-doped low mobility graphene at mid-IR wavelengths. Figure 8 shows that large LDOS and Purcell factor enhancements are predicted for these parameters. The Purcell factor is 2 orders of magnitude less than for the high-mobility graphene in the THz regime; this is partially attributable to the ratio of z/λ which is larger for mid-IR wavelengths. The Purcell factor remains, however, improved over that of the metal/dielectric HMM. We observe a crossover between wavelengths of 3 and 5 μm (177 and 248 meV) indicated by the much slower decay of the LDOS and Purcell factor with z. We attribute this crossover to the transition from elliptical to hyperbolic isofrequency contour.[14] A simple Bloch theory[52] for an infinite graphene-based metamaterial[22]

shows that the transition from an effective permittivity $\epsilon_{\parallel} > 0$ to $\epsilon_{\parallel} < 0$ should occur in exactly this regime, while $\epsilon_{\perp}$ remains positive.

We should stress here the non-negligible role of loss in the enhancement of the Purcell factor. A lossy material need not be hyperbolic in order to produce a large Purcell enhancement: for example, the metallic film in the inset of Fig. 6 has a larger Purcell enhancement than a metal/dielectric HMM at small enough distances. For hyperbolic systems, instead we see an enhanced Purcell coefficient over a longer distance.

IV. SUMMARY

In conclusion, we have found that thin graphene stacks are HMMs in the THz to mid-infrared regime for a wide range of parameters. We have studied the high-k propagating modes as well as the wave-vector-resolved local density of states for graphene stacks and find an enhancement of both quantities at wave vectors that are evanescent in vacuum. This implies that enhanced near-field effects including subwavelength imaging and confinement of light may be possible. We also calculate the Purcell factor for both our graphene HMMs, and HMMs composed of metal/dielectric stacks. We find that the graphene HMMs perform very well compared to this benchmark at both the THz and mid-IR wavelengths. The frequency range of the graphene HMM is limited by the Fermi energy, $\hbar\omega \lesssim \varepsilon_F$, and so the graphene must be highly doped for mid-IR applications. We observe a transition from high Purcell enhancement to low Purcell enhancement around 3–5 μm for the low-mobility, highly doped graphene, which we attribute to a transition from a hyperbolic to an elliptical isofrequency contour.

ACKNOWLEDGMENTS

Work at the University of Texas was supported by the Welch foundation under grant TBF1473 and the DOE Division of Materials Sciences and Engineering under grant DE-FG03-02ER45958. Michigan researchers were supported by the NSF MRSEC program under DMR 1120923.

[1] D. R. Smith and D. Schurig, Phys. Rev. Lett. **90**, 077405 (2003).
[2] I. V. Lindell, S. A. Tretyakov, K. I. Nikoskinen, and S. Ilvonen, Microwave Opt. Tech. Lett. **31**, 129-133 (2001).
[3] I. I. Smolyaninov and E. E. Narimanov, Phys. Rev. Lett. **105**, 067402 (2010).
[4] Z. Jacob, I. Smolyaninov, and E. Narimanov, Appl. Phys. Lett. **100**, 181105 (2012).
[5] Z. Jacob, J. Y. Kim, G. V. Naik, A. Boltasseva, E. E. Narimanov, and V. M. Shalaev, Appl. Phys. B **100**, 215 (2010).
[6] A. Fang, T. Koschny, and C. M. Soukoulis, Phys. Rev. B **79**, 245127 (2009).
[7] O. Kidwai, S. V. Zhukovsky, and J. E. Sipe, Phys. Rev. A **85**, 053842 (2012).
[8] A. V. Kildishev and V. M. Shalaev, Opt. Lett. **33**, 43 (2008).
[9] A. A. Govyadinov and V. A. Podolskiy, Phys. Rev. B **73**, 155108 (2006).
[10] I. I. Smolyaninov, Y.-J. Hung, and C. C. Davis, Science **315**, 1699 (2007).
[11] Z. Liu, H. Lee, Y. Xiong, C. Sun, and X. Zhang, Science **315**, 1686 (2007).
[12] Y. Guo, C. L. Cortes, S. Molesky, and Z. Jacob, Appl. Phys. Lett. **101**, 131106 (2012).
[13] J. Kim, V. P. Drachev, Z. Jacob, G. V. Naik, A. Boltasseva, E. E. Narimanov, and V. M. Shalaev, Opt. Express **20**, 8100 (2012).
[14] H. N. S. Krishnamoorthy, Z. Jacob, E. Narimanov, I. Kretzschmar, and V. M. Menon, Science **336**, 205 (2012).
[15] T. U. Tumkur, L. Gu, J. K. Kitur, E. E. Narimanov, and M. A. Noginov, Appl. Phys. Lett. **100**, 161103 (2012).
[16] J. Kanungo and J. Schilling, Appl. Phys. Lett. **97**, 021903 (2010).
[17] L. Ju, B. Geng, J. Horng, C. Girit, M. Martin, Z. Hao, H. A. Bechtel, X. Liang, A. Zettl, Y. R. Shen, and F. Wang, Nat. Nanotechnol. **6**, 630 (2011).
[18] Q. Bao and K. P. Loh, ACS Nano **6**, 3677 (2012).
[19] A. N. Grigorenko, M. Polini, and K. S. Novoselov, Nat. Photon. **6**, 749 (2012).
[20] H. Yan, X. Li, B. Chandra, G. Tulevski, Y. Wu, M. Freitag, W. Zhu, P. Avouris, and F. Xia, Nat. Nanotechnol. **7**, 330 (2012).
[21] Y. V. Bludov, A. Ferreira, N. M. R. Peres, and M. I. Vasilevskiy, Int. J. Mod. Phys. B **27**, 1341001 (2013).
[22] I. V. Iorsh, I. S. Mukhin, I. V. Shadrivov, P. A. Belov, and Y. S. Kivshar, Phys. Rev. B **87**, 075416 (2013).
[23] A. Andryieuski, A. V. Lavrinenko, and D. N. Chigrin, Phys. Rev. B **86**, 121108 (2012).
[24] M. A. K. Othman, C. Guclu, and F. Capolino, Opt. Express **21**, 7614 (2013).
[25] A. DaSilva and A. MacDonald, contributed talk at *the APS March Meeting, Baltimore, MD, March 18–22, 2013* (unpublished).
[26] K. S. Novoselov, A. K. Geim, S. V. Morozov, D. Jiang, Y. Zhang, S. V. Dubonos, I. V. Grigorieva, and A. A. Firsov, Science **306**, 666 (2004).
[27] S. S. Datta, D. R. Strachan, E. J. Mele, and A. T. C. Johnson, Nano Lett. **9**, 7 (2009).
[28] D. Sun, C. Divin, C. Berger, W. A. de Heer, P. N. First, and T. B. Norris, Phys. Rev. Lett. **104**, 136802 (2010).
[29] T. Ohta, A. Bostwick, T. Seyller, K. Horn, and E. Rotenberg, Science **313**, 951 (2006).
[30] J.-H. Chen, C. Jang, S. Adam, M. S. Fuhrer, E. D. Williams, and M. Ishigami, Nat. Phys. **4**, 377 (2008).
[31] K. Joulain, R. Carminati, J.-P. Mulet, and J.-J. Greffet, Phys. Rev. B **68**, 245405 (2003).
[32] G. S. Agarwal, Phys. Rev. A **11**, 253 (1975).
[33] C. Girard, Rep. Prog. Phys. **68**, 1883 (2005).
[34] E. H. Hwang and S. Das Sarma, Phys. Rev. B **75**, 205418 (2007).
[35] L. A. Falkovsky and S. S. Pershoguba, Phys. Rev. B **76**, 153410 (2007).
[36] T. Stauber, N. M. R. Peres, and A. K. Geim, Phys. Rev. B **78**, 085432 (2008).
[37] K. F. Mak, M. Y. Sfeir, Y. Wu, C. H. Lui, J. A. Misewich, and T. F. Heinz, Phys. Rev. Lett. **101**, 196405 (2008).

[38]S. H. Abedinpour, G. Vignale, A. Principi, M. Polini, W.-K. Tse, and A. H. MacDonald, Phys. Rev. B **84**, 045429 (2011).
[39]M. Jablan, H. Buljan, and M. Soljacic, Phys. Rev. B **80**, 245435 (2009).
[40]F. H. L. Koppens, D. E. Chang, and F. J. Garcia de Abajo, Nano Lett. **11**, 3370 (2011).
[41]O. Kidwai, S. V. Zhukovsky, and J. E. Sipe, Opt. Lett. **36**, 2530 (2011).
[42]C. L. Cortes, W. Newman, S. Molesky, and Z. Jacob, Jpn. J. Opt. **14**, 063001 (2012).
[43]Kenneth W.-K. Shung, Phys. Rev. B **34**, 979 (1986).
[44]D. Olego, A. Pinczuk, A. C. Gossard, and W. Wiegmann, Phys. Rev. B **25**, 7867 (1982).
[45]S. Das Sarma and J. J. Quinn, Phys. Rev. B **25**, 7603 (1982).
[46]J. K. Jain and P. B. Allen, Phys. Rev. Lett. **54**, 2437 (1985).
[47]A. Pinczuk, M. G. Lamont, and A. C. Gossard, Phys. Rev. Lett. **56**, 2092 (1986).
[48]G. F. Giuliani and J. J. Quinn, Phys. Rev. Lett. **51**, 919 (1983).
[49]W. Yan, M. Wubs, and N. A. Mortensen, Phys. Rev. B **86**, 205429 (2012).
[50]A. F. da Silva, I. Pepe, C. Persson, J. S. de Almeida, C. M. Araújo, R. Ahuja, B. Johansson, C. Y. An, and J.-H. Guo, Phys. Scr. **2004**, 180 (2004).
[51]P. B. Johnson and R. W. Christy, Phys. Rev. B **6**, 4370 (1972).
[52]N. C. Constantinou and M. G. Cottam, J. Phys. C **19**, 739 (1986).